Electronic structure of the surface unoccupied band of Ge(001)-$c(4 \times 2)$: Direct imaging of surface electron relaxation pathways

J. Kanasaki*
The Institute of Scientific and Industrial Research, Osaka University, Mihogaoka 8-1, Ibaraki, Osaka 567-0047, Japan

I. Yamamoto and J. Azuma
Synchrotron Light Application Center, Saga University, Yayoigaoka 8-7, Tosu, Saga 841-0005, Japan

S. Fukatsu
Graduate School of Arts and Sciences, University of Tokyo, Komaba 3-8-1, Meguro, Tokyo 153–8902, Japan
(Received 9 May 2017; revised manuscript received 11 August 2017; published 1 September 2017)

We have studied the electronic structure of the surface unoccupied band (SUB) of clean Ge(001)-$c(4 \times 2)$, with high energy and momentum resolution, by means of time- and angle-resolved two-photon photoelectron spectroscopy. The time evolution of photoelectron intensity images, measured as functions of energy and emission angle after photoexcitation with laser pulses (1.5 eV, 200 fs), provides a momentum space view of the relaxation pathways of surface excited electrons toward the bottom of the SUB. Surface excited electrons relax in several picoseconds along the strongly dispersive directions ($\bar{\Gamma}\overline{J'}$ and $\bar{\Gamma}\overline{J_2'}$) and then accumulate near the band bottom. Taking into account the ultrafast change of surface potential, possibly due to the spatial redistribution of nonthermal carriers generated by photoexcitation, an energy width of 0.22 eV was determined as the surface band gap, as well as the surface dispersion properties along three high-symmetry directions.

DOI: 10.1103/PhysRevB.96.115301

I. INTRODUCTION

Group-IV semiconductor (001) surfaces are one model system for fundamental and applied surface science, and extensive studies have been conducted to elucidate their geometric and electronic properties. The atomic structures of Si(001) and Ge(001) surfaces are characterized by the dimer-row structure of the outermost atomic layer, where surface atoms located in neighboring rows are dimerized and the dimers thus formed are aligned parallel to the [110] and [−110] directions to show double-domain reconstructions separated by single-layer steps [1]. The surface dimer atoms are buckled to form a semiconductor-type surface electronic structure: the s-like orbitals on the upper dimer atoms form an occupied surface band around the top of the valence band, while the p_z-like orbitals on the lower dimer-atoms form a π^*-bonded surface unoccupied band (SUB). This quasi-one-dimensional nature manifests itself in the anisotropic electronic properties; dispersions of the surface occupied and unoccupied bands are large along the $\bar{\Gamma}\overline{J'}$ direction of the surface Brillouin zone, but small along the $\bar{\Gamma}\bar{J}$ direction. The structure of the surface valence band has been revealed experimentally by angle-resolved photoemission spectroscopy (ARPES), and the results have been compared with those calculated based on the geometries of the reconstructed surface [2,3]. The top of the surface valence band is located just below the bulk band edge, thereby forming resonant states around the $\bar{\Gamma}$ point. Similarly, the structure of the SUB has been studied extensively by several experimental techniques and theoretical calculations. Nevertheless, controversies remain in terms of fundamental properties of the SUB, including the width of the bands, energy dispersion properties, and the energy position of the band edge.

ARPES has also been used to study the electronic structures of the SUB of Ge(001) surfaces [4,5]. In these studies, the population of thermally excited electrons in the SUB was analyzed statistically for a wide range of sample temperatures, and the surface band gap was determined to be 0.3 eV. Nakatsuji *et al.* revealed the dispersion property of the low-lying surface unoccupied states along the $\bar{\Gamma}\bar{J}$ direction. However, this technique is not suitable for the mapping of higher-lying electronic states because the thermal energy is insufficient for electrons to populate states with large excess energies. In addition, heating of the surfaces enhances the flip-flop motion of surface dimer atoms and transforms the most stable $c(4 \times 2)$ phase into the 2×1 (1×2) phase [1]. Although the measured surface band gap for the high-temperature phase is in agreement with that of the low-temperature phase determined by scanning tunneling spectroscopy (STS) [6–8], the phase transformation can change the dispersion properties of surface electronic bands. Recently, two research groups separately analyzed the surface standing waves of electrons injected by scanning tunneling microscopy (STM) [4,9] and revealed a 1-eV-wide dispersion along the $\bar{\Gamma}\overline{J'}$ direction in the low-temperature phase, which was larger than the calculated results [2,3,10,11]. However, the use of this technique is strictly limited to this direction since the standing waves are formed only in the direction of the dimer row.

In these respects, angle-resolved inverse photoemission spectroscopy (IPES) seems a better technique to study the whole picture of the unoccupied surface band structure. IPES involves directing a collimated low-energy electron beam to the surface to generate photons when the incident electrons decay to lower-lying unoccupied states. Angle-resolved IPES studies have determined the structure of the SUB, in which the bottom of the SUB is located at 0.6–0.8 eV above the valence-

*Corresponding author: kanasaki@sanken.osaka-u.ac.jp

band top and the bandwidth is about 0.5 eV [12,13]. However, these results are not entirely consistent with those obtained by other experimental techniques. Thus there are several discrepancies and technical limitations in previous studies. Therefore knowledge regarding the electronic structures of the SUB still needs to be improved to a level comparable with that for the surface valence band in order to gain a complete picture of the surface band structure.

Here, we determine the electronic structure of the SUB of the clean Ge(001)-$c(4 \times 2)$ surface, with high energy and momentum resolution, by means of time- and angle-resolved two-photon photoelectron spectroscopy (2PPE). Although the 2PPE technique has generally been used to study the ultrafast dynamics of photoexcited electrons in unoccupied bands [14–18], it allows also imaging of the electronic structures of unoccupied bands by tracing the relaxation pathways of excited electrons. In this study, excited electrons are injected with 1.5-eV pump laser pulses, and subsequent electron dynamics within the SUB are probed with fourth-harmonic (6.0 eV) pulses with changing the time delay between the pump and probe pulses. It has been shown that surface electrons relax to the band edge and accumulate near the band bottom within several picoseconds. Based on the imaged relaxation pathways, the energy dispersion properties of the SUB along three high-symmetry directions and the surface band gap energy are accurately determined.

II. EXPERIMENTAL DETAILS

All experiments were conducted using the Saga University Beamline BL13 at the Saga Light Source. Specimens $15 \times 3 \times 0.5\,\mathrm{mm}^3$ in size were cut from a p-doped Ge(001) wafer (0.25 Ω cm). Clean surfaces were obtained by repeated cycles of sputtering with 1-keV Ne ions followed by annealing at 700 °C in an ultrahigh-vacuum chamber. After the cleaning procedure, the surface exhibited double domains of a dimer-row structure, showing an overlapped (2×1) and (1×2) low-energy electron diffraction pattern at room temperature. With low-temperature STM, we separately confirmed that the surface thus prepared transformed into the double domains of $c(4 \times 2)$ and $c(2 \times 4)$ phases by cooling to the liquid nitrogen temperature. Passivation of dangling bonds was performed by exposing the surface to atomic hydrogen of 1 langmuir at a sample temperature of 250 °C [19]. The clean and H-terminated samples were transferred to the analyzing chamber and kept at 10 K throughout the measurements.

In 2PPE spectroscopic measurements, pump laser pulses ($h\nu = 1.5$ eV, s-pol.) of 200-fs temporal width and their fourth harmonic probe pulses (6.0 eV, p-pol.) were generated at a repetition rate of 100 kHz from a Ti:sapphire laser source (Coherent Mira-900F & RegA-9000). The pump and probe pulses were incident collinearly on the same spot of the surface at an incident angle of 55°. The origin of the time delay ($t_\mathrm{d} = 0$) was determined based on the cross correlation profile between the pump and probe laser pulses by detecting photoelectrons. The emitted photoelectrons were analyzed using a hemispherical electrostatic analyzer (MB Scientific, A-1) equipped with a 2D-CCD counting detector, which provided two-dimensional images of the photoelectron intensity I as functions of kinetic energy and of emission angle θ measured from the surface normal in the plane perpendicular to the optical plane and the sample surface. The acceptance angle of the analyzer is ±15° from the surface normal. Angle-resolved measurements for the Ge(001) surfaces were conducted along the $\bar{\Gamma}\bar{J}$ ($\bar{\Gamma}\bar{J'}$) directions ($\varphi = 0°$) and the $\bar{\Gamma}\bar{J'_2}$ direction ($\varphi = 45°$), as described below. The energy position of the Fermi level (E_F) was determined using Au before and after the 2PPE measurements. The overall energy and time resolution of the system was 45 meV and 600 fs, respectively.

III. RESULTS

Figures 1(a)–1(f) show the logarithmic images of the photoelectron intensity I, probed at several different delay times, as functions of kinetic energy ε relative to E_F and θ for a clean Ge(001) surface. The experimental geometry is shown in Fig. 1(g). The images were obtained with the sample placed at the azimuthal angle $\varphi = 0°$, where the detection plane includes the ⟨001⟩ crystallographic axis along the surface normal and the ⟨110⟩ axis. Since the (001) surface consists of two domains that are rotated by 90°, the abscissa (θ) corresponds to the $\bar{\Gamma}\bar{J}$ and $\bar{\Gamma}\bar{J'}$ directions in the momentum space, as shown in Figs. 1(h) and 1(i).

In Fig. 1(a) ($t_\mathrm{d} = -5$ ps), a structure is observed in the energy range of $\varepsilon < 0.1$ eV, where photoelectrons form the structure with downward dispersion as θ increases. Since the Fermi level on this surface is pinned near the top of the bulk valence band, the observed structure is possibly due to the electrons emitted from the valence band. A group of electrons are also seen in the energy range between 0.2 and 0.4 eV, corresponding to the bulk band gap region. The electrons in the gap region were detected only when the surface was repeatedly excited with the pump laser pulses. We also found that the intensity was reduced significantly by hydrogen termination. Therefore the photoelectrons emitted from the gap region reflect the population of photoexcited electrons in the SUB of the Ge(001)-$c(4 \times 2)$. Since the surface was illuminated repeatedly at 100 kHz, Fig. 1(a) corresponds to the images of states populated by electrons at 10 μsec after the previous pump pulse. Thus the observed group of electrons could be ascribed to the long-lived photoexcited electrons near the bottom of the SUB, which were injected by the previous pump excitation.

The relaxation pathways in the SUB are clearly shown in the time series photoelectron images. At $t_\mathrm{d} \geqslant 0$ [Figs. 1(b)–1(f)], two structures are visible in the images: the first is the structure with little energy dispersion located near the bottom of the SUB, and the second is the structure with large energy dispersion, extending from the bottom ($\varepsilon = 0.2$ eV) to $\varepsilon = 1.2$ eV at $\theta = 25°$. Compared to the band structure reported previously [4], the former indicates the temporarily occupied electronic states along the $\bar{\Gamma}\bar{J}$ direction, while the latter shows those along the $\bar{\Gamma}\bar{J'}$ direction. Figure 1(b) ($t_\mathrm{d} = 0$ ps) shows the population of excited electrons in the SUB just after photoexcitation: excited electrons distribute in the states along the $\bar{\Gamma}\bar{J'}$ line up to $\varepsilon = 1.2$ eV as well as in the states along the $\bar{\Gamma}\bar{J}$ line. As t_d increases, the excited surface electrons relax and most electrons eventually accumulate near the band bottom ($\theta = 0$) and in states along the $\bar{\Gamma}\bar{J}$ line, the energies of which are located near the bottom [Fig. 1(f)]. The intensity

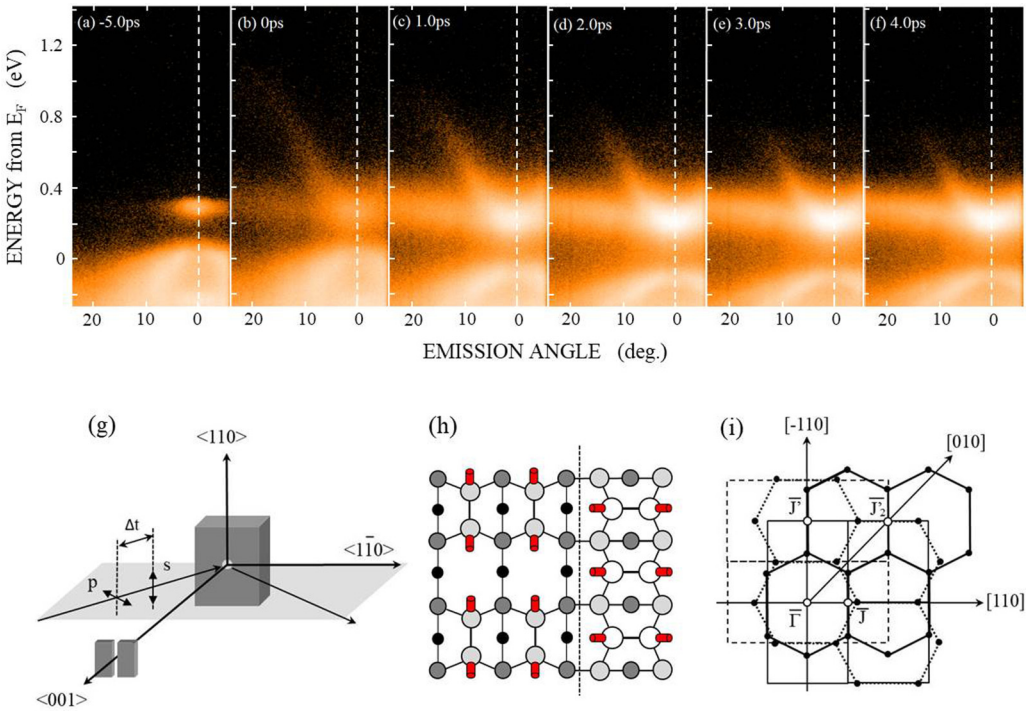

FIG. 1. Logarithmic images $I(\varepsilon, \theta)$ for clean Ge(001)-$c(4 \times 2)$ probed at (a) -5, (b) 0, (c) 1, (d) 2, (e) 3, and (f) 4 ps after the pump laser pulses. The experimental geometry is shown in (g). The measurements were carried out with the azimuthal angle of the specimen kept at $\varphi = 0^\circ$, corresponding to the $\bar{\Gamma}\bar{J}$ and $\bar{\Gamma}\overline{J'}$ directions. Surface atomic arrangements and the SBZs of two domains separated by a single atomic step are shown in (h) and (i).

at the band bottom gets stronger to reach a maximum at 4 ps after excitation, as described below.

Similar measurements were performed for $\varphi = 45^\circ$, where the detection plane corresponds to the $\bar{\Gamma}\overline{J_2'}$ direction in the momentum space for the two domains on the surface [Figs. 2(h) and 2(i)]. The time series images are shown in Figs. 2(a)–2(f). As in the case of $\varphi = 0^\circ$, long-lived excited electrons are observed near the band bottom at negative delay times. However, only one largely-dispersive structure was imaged after excitation extending from the bottom at the $\bar{\Gamma}$ point ($\theta = 0$). Since the bottom energy agrees with that for $\varphi = 0^\circ$, the observed structure shows the dispersion for the same SUB but along a different direction. At $t_d = 0$, excited surface electrons distribute up to the states with excess energy as high as 1.2 eV. Higher-lying electrons disappear in a few picoseconds, and the population around the band bottom increases accordingly.

We acquired the photoelectron images $I(\varepsilon, \theta)$ for the two azimuthal angles at the delay times from -1 ps to 4 ps with an interval of 0.2 ps. Figure 3(a) shows the temporal changes of angle-integrated electron distributions, each of which was obtained by integrating the corresponding $I(\varepsilon, \theta)$ for $\varphi = 0^\circ$ over the range of $-10^\circ < \theta < 10^\circ$. The broken line indicates the spectrum without the pump pulse, which shows no structure above the top of the valence band. At $t_d = -1$ ps, corresponding to 10 μs after the previous pump excitation, the long-lived excited electrons form a peak near $\varepsilon = 0.25$ eV. The electron population grows gradually after excitation, reaching a maximum at 4 ps. In response to the growth of the excited electron population, the intensity of the valence band changes: the intensity just below the top edge apparently increases, while the intensity at the energy region between -0.25 and -0.1 eV relative to the valence-band edge decreases slightly to form a dip in the distribution. We also found that the surface occupied states distribute in the same energy region based on the reduction of the intensity by passivation with hydrogen atoms. Therefore the population of photoexcited holes in the surface resonance states could be responsible for the reduction in photoelectron intensity. Another structure, designated as B around 0.3 eV below the valence-band edge, is visible in all the spectra. This structure B is likely due to bulk-originated states, because its intensity is unchanged even if the surface is terminated with hydrogen.

An intriguing point in Fig. 3(a) is the significant energy shift of the spectra towards the lower energy side as t_d increases. In general, the surface potential (SP) of a semiconductor is changed by photoillumination [1]. The magnitude of the energy shift ΔE is measured by that of peak B relative to the peak position under the unpumped condition. In order to clarify the temporal change of SP by the pump pulses, we plot ΔE as a function of t_d in Fig. 3(b). It is possible to divide two time regions with regard to the behavior of ΔE: (I) ΔE decreases rapidly from the initial value in the first 500 fs and reaches the minimum at -85 meV around $t_d = 2$ ps; (II) ΔE then increases slowly and crosses zero around 100 ps. Although the change of ΔE is not plotted in the time region beyond 10^3 ps, ΔE continues to increase slowly, and eventually returns to $+35$ meV when the next pump pulse arrives.

The black and red solid lines in Fig. 3(c) show the emission spectra measured with probe laser pulses only and with (pump

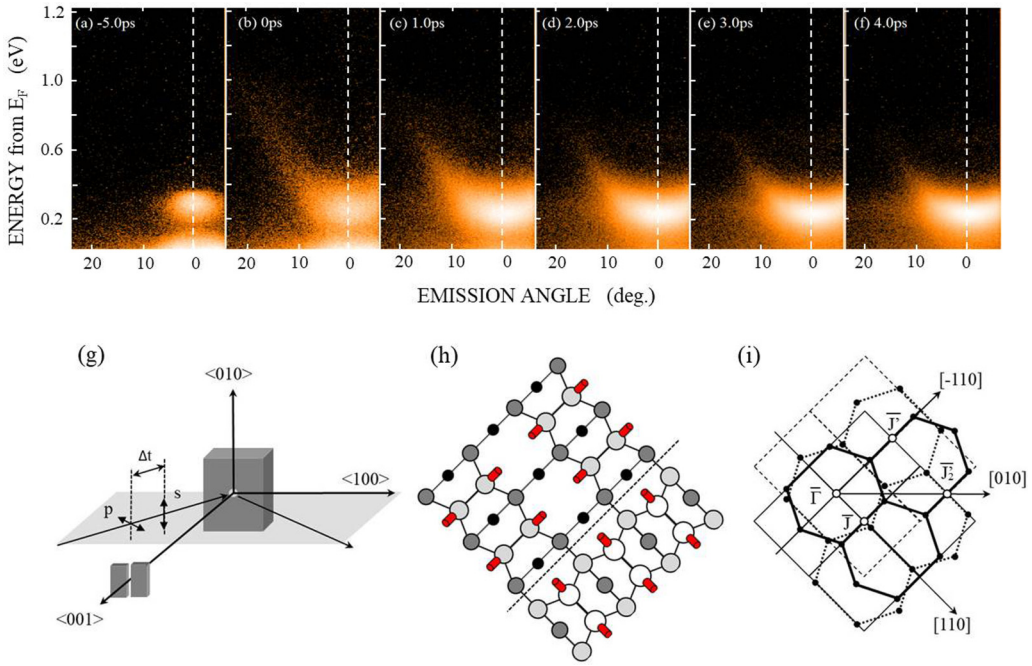

FIG. 2. Logarithmic images $I(\varepsilon, \theta)$ for clean Ge(001)-$c(4 \times 2)$ probed at (a) -5, (b) 0, (c) 1, (d) 2, (e) 3, and (f) 4 ps after the pump laser pulses. The experimental geometry is shown in (g). The measurements were carried out with the azimuthal angle of the specimen kept at $\varphi = 45°$, corresponding to the $\bar{\Gamma}\,\overline{J'_2}$ directions. Surface atomic arrangements and the SBZs are shown in (h) and (i).

+ probe) laser pulses at $t_d = -1$ ps, respectively. In order to compensate ΔE of SP induced by pump pulses, the latter spectrum is shifted toward the lower energy sides by 35 meV, so that the locations of the B structure coincide. The change of overall structure in the valence-band region is small, except for the slight increase of intensity at the higher energy side of the structure B (-0.3 to -0.2 eV). Although the slope of the valence-band edge is gentler under illumination, the energy position at half-maximum intensity agrees with each other, which we regard as the valence-band-top energy. In

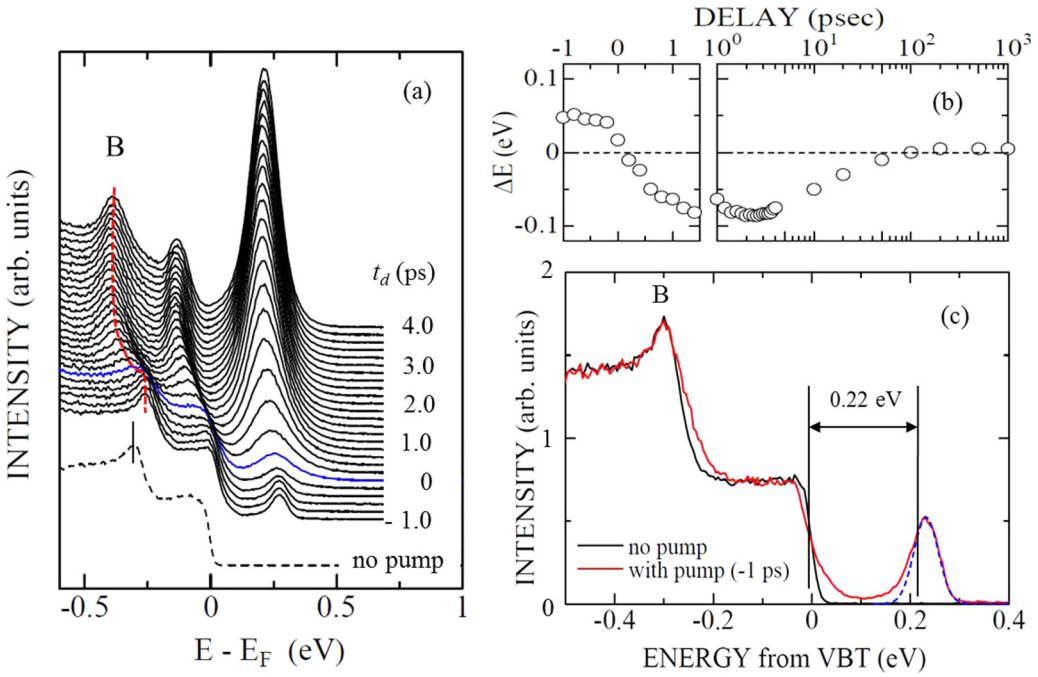

FIG. 3. (a) Angle-integrated spectra acquired at several delay times between the pump and probe laser pulses; the spectrum without pump laser pulse is shown for comparison. (b) The photoinduced energy shift ΔE of the spectra is plotted as a function of delay time. The magnitude of ΔE is given by the energy shift of the bulk-originating structure, B. (c) Angle-integrated spectra with and without pump laser pulses. The spectrum acquired at -1 ps is shifted by ΔE to account for the photoinduced change of the surface potential.

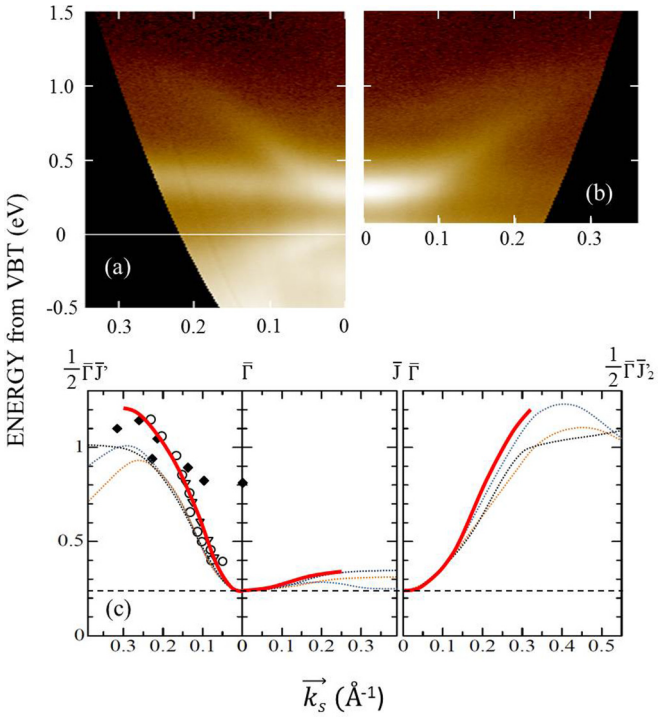

FIG. 4. Relaxation pathways of the surface electrons on Ge(001)-$c(4 \times 2)$ surface imaged in $(\varepsilon', \vec{k_s})$ space, derived from the time evolution of photoelectron images measured at (a) $\varphi = 0^\circ$ and (b) 45°. Each image is obtained by integrating $I(\varepsilon, \theta)$ acquired every 200 fs from $t_d = 0$ to 1.5 ps, taking the dynamical change of surface potential into account. (c) Energy dispersion relations of the SUB along the three high-symmetry directions are depicted by red solid lines. Circles, triangles, and diamonds indicate the previous experimental data from Refs. [4], [9], and [12], respectively; orange, black, and blue dotted lines show the calculated bands from Refs. [2], [4], and [10], respectively.

contrast, a prominent peak is formed at 0.25 eV by pump lasers due to the population of long-lived surface electrons at the bottom of the SUB. The dotted line indicates the best fit of the population in the SUB, using the Maxwell-Boltzmann distribution at $T = 10$ K convoluted by Gaussian functions with an energy width of 45 meV. The observed population was successfully described when we locate the bottom energy of SUB at 0.22 eV above the valence-band top.

Tracing the temporal change of electron populations, we depict the relaxation pathways of surface electrons in the $(\varepsilon', \vec{k_s})$ space, where ε' is the energy relative to the top of the valence band and $\vec{k_s}$ is the wave vector parallel to the surface. In order to determine the pathways during the relaxation exactly, the dynamical change of SP [Fig. 3(b)] should be taken into account. We shifted each image by ΔE at the corresponding delay time, and then integrated the images measured from 0 to 1.5 ps. Figures 4(a) and 4(b) show the results obtained from the integrated images. Three distinct relaxation pathways are clearly imaged merging together at the bottom ($\bar{\Gamma}$ point); two of the paths are imaged along the $\langle 110 \rangle$ and $\langle -110 \rangle$ directions, Fig. 4(a), and the other along the $\langle 010 \rangle$ direction, Fig. 4(b). In addition to the three dispersion structures of the SUB, a weakly dispersive structure is found from 0.85 eV ($k_s = 0$ Å^{-1}) to 1.2 eV ($k_s = 0.25$ Å^{-1}) above the valence-band top. The energy at the $\bar{\Gamma}$ point is in good agreement with that at the local minimum in the X valley. Thus this structure can be ascribed to the relaxation pathway for bulk excited electrons in the X valley, as will be reported elsewhere [20].

The results of band mapping based on the relaxation pathways of surface electrons on the $c(4 \times 2)$ phase are summarized in Fig. 4(c), in which the red solid lines indicate the measured band diagram depicted as a function of the wave number along the three high-symmetry directions. The dispersion is largest along the $\bar{\Gamma}\overline{J'}$ direction: ε' increases steeply from the band bottom, 0.22 eV above the valence-band top at the $\bar{\Gamma}$ point, and exceeds 1.2 eV at $k_s = 0.3$ Å^{-1}. The first experimentally determined data for two other symmetric directions, $\bar{\Gamma}\bar{J}$ and $\bar{\Gamma}\overline{J'_2}$, are also shown in the figure. The energy along the $\bar{\Gamma}\overline{J'_2}$ direction increases a little more slowly as compared to the $\bar{\Gamma}\overline{J'}$ direction, but exceeds 1.2 eV when k_s reaches 0.3 Å^{-1}. In contrast to these two directions, the energy dispersion along the $\bar{\Gamma}\bar{J}$ direction is fairly small and the width is at most 0.15 eV at the middle point of the zone edge.

IV. DISCUSSION

Extensive studies have been carried out to determine both the surface band gap and energy dispersion properties as important factors for characterizing the electronic band structure of the Ge(001) surface. The width of the surface band gap of the $c(4 \times 2)$ phase has been measured based on the results of local densities of surface states by STS. Several research groups have determined the surface gap energy to be 0.2–0.3 eV for the low temperature phase [6–8]. Nakatsuji *et al.* measured the electron density at the bottom of the SUB as a function of sample temperature using conventional ARPES [4]. They analyzed the population of thermally excited electrons using the Boltzmann distribution at different temperatures, and determined the gap energy to be 0.3 eV. Although their measurements were carried out in a wide temperature range above room temperature, the observed gap energy was comparable to that for the low temperature phase measured by STS. As already mentioned, we analyzed the distribution of photoexcited electrons near the bottom of the SUB and determined the surface gap energy to be 0.22 eV, which is in reasonable agreement with these previous studies. In contrast, Kipp *et al.* and Ortega *et al.* measured the width of the surface band gap by combining the ARPES and angle-resolved IPES, and determined it to be 0.6–0.8 eV at the $\bar{\Gamma}$ point [12,13]. The reported gap energy is significantly larger than other experimental results, while the width of dispersion is smaller as indicated by diamonds in Fig. 4(c). The difference may be ascribed to a poor energy resolution of their measurements or to the incorrect identification of the bottom of the lowest SUB; the reported gap energy is comparable to the energy separation between the valence band and the unoccupied dimer-bond band, which forms the second lowest SUB [4,11].

The results of band mapping reported previously are summarized in Fig. 4(c), together with the present result. Two STM research groups obtained the dispersion relation of

the SUB along the $\bar{\Gamma}\overline{J'}$ direction by analyzing the oscillation of the standing wave formed by injected surface electrons at the atomic steps [4,9]. Their results are indicated by the open circles and the triangles, respectively, in the figure; the width of the band along the $\bar{\Gamma}\overline{J'}$ direction is larger than 1 eV. These dispersion data for the $c(4 \times 2)$ phase coincide very well with our results in the k region between the $\bar{\Gamma}$ point and $0.3\,\text{Å}^{-1}$. The technique used in Refs. [4,9] is applicable to the band mapping only along the $\bar{\Gamma}\overline{J'}$ direction because the standing wave is formed exclusively along the dimer rows. In contrast, our technique can provide the energy dispersion relations along any directions in the surface Brillouin zone by measuring photoelectron intensity maps with changing φ. No other experimental data along the $\bar{\Gamma}\bar{J}$ and $\bar{\Gamma}\overline{J'_2}$ directions are available, but some calculated data have been provided. The broken lines represent the calculated results [2,4,10], the energies of which are shifted to coincide with the bottom energy of the SUB. It is evident that the overall behavior is similar but the calculated results tend to show a slightly smaller dispersion, compared to the experimental data.

As with the Ge(001) surface, the geometric structure of the low temperature Si(001) surface is characterized by a $c(4 \times 2)$ structure formed by asymmetric dimers. The geometric similarity between the two surfaces shows a marked resemblance in electronic band structure. Weinelt *et al.* reported the electronic structure and ultrafast electron dynamics on Si(001)-$c(4 \times 2)$ at 90 K measured by angle- and time-resolved 2PPE [15]. The authors revealed a strong dispersion of the SUB along the dimer rows extending from the band minimum at $\bar{\Gamma}$ point, while little dispersion along the dimer-bond direction. They also found a band with nearly no energy dispersion, X band, about 130 meV below the bottom of the SUB, and assigned it to the surface exciton band. According to their report, the X band plays important roles in the electron dynamics on the surface; surface excited electrons accumulate at the band bottom in 1.5 ps, and then relax within 5 ps with excited holes to form a surface exciton that exists for nanoseconds. In spite of the similarities of structural and electronic structures between the two surfaces, no band like the X band has been found below the SUB on the Ge(001)-$c(4 \times 2)$ surface. Surface excited electrons on Ge(001) relax to the bottom of the SUB in a few picoseconds and stay there; some excited electrons survive near the band bottom over 10 μs after excitation.

The present study demonstrates the nascent population of electrons with a broad range of energies and the subsequent slow accumulation of excited electrons in the SUB. In view of the photon energy of the pump laser pulses that is larger than the bulk direct gap at the Γ point as well as the surface band gap, there are two possible paths for injecting electrons into the SUB. The first is the direct optical transitions to the SUB and the other is the bulk transitions followed by the bulk-to-surface transfer of excited electrons. Wormeester *et al.* studied the surface optical properties on Ge(001)-2 × 1 using normal incidence ellipsometry, and found an absorption band centered around 1.4 eV [21]. They ascribed this structure to the surface optical transitions between the occupied and unoccupied dangling-bond bands, based on the symmetries and the joint density of states of the two surface bands. Thus the pump pulses we used can directly populate the upper edge of the SUB with photoexcited electrons.

In addition to direct injection, illumination induces optical transitions from the heavy-hole (hh), light-hole (lh), and split-off (so) valence bands to the Γ valley of the bulk conduction band. Based on the bulk band structure [22], the final state energies of bulk transitions by 1.5-eV photons are predicted to be 0.66, 0.58, and 0.31 eV, respectively, above the conduction band minimum. In fact, 2PPE experiments using the third harmonic (4.5 eV, p-pol.) probe light have revealed that the photoexcitation really generates the three packets of excited electrons with the predicted excess energies in the Γ-valley of the bulk conduction band [20]. Due to the energy overlap between the bulk and surface electronic bands, the bulk-to-surface transfer can take place, which is similar to what was observed on the Si(001) surface [15,17]. The slow increase of the electron population in a few picoseconds strongly indicates an important role of the indirect electron injection. Thus it is likely that the observed temporal change in electron population in the SUB can be attributed to the two paths: the direct surface transitions and the indirect inflow via the bulk-to-surface transfer following bulk direct transitions.

An additional intriguing finding from the present study is the significant change in SP induced within a few picoseconds after photoexcitation. In general, photogenerated electrons and holes move across the space charge region and their spatial distribution determines the position of SP relative to the bulk Fermi level. As shown in Fig. 3(b), the temporal change of SP is characterized by two time regimes: the SP moves downward in the first 500 fs after photoexcitation to reach the minimum of ΔE (−85 meV) around $t_\text{d} = 2$ ps, and then slowly returns to $\Delta E = +35$ meV over a nanosecond time scale. Since it takes several picoseconds for the photoinjected electron-hole system to be thermalized at the band edges [14–18,23], the downward shift of SP clearly takes place before the thermalization of excited carriers is completed. Thus the transport of nonthermal carriers plays an important role in the ultrafast movement of SP, while the slow return over a longer-time scale can be governed by the transport of thermalized carriers across the space charge region.

The optical excitation forms the nascent Γ-valley population, far from equilibrium, of electrons and holes in the bulk conduction and valence bands, respectively. The relationship between the excess energies given to excited electrons and holes in the direct band-to-band transitions can be described by $E_\text{ex}(\text{e}) + E_\text{ex}(\text{h}) + E_\text{g}(\Gamma) = h\nu$, where $E_\text{ex}(\text{e})$ and $E_\text{ex}(\text{h})$ are the excess energies of excited electrons and holes respectively measured from the Γ-valley conduction and valence-band edges and $E_\text{g}(\Gamma)$ is the energy separation at the Γ point between the bulk valence and conduction bands. Three optical transition channels from the hh, lh, and so valence bands form three packets of excited electrons in the Γ valley of the bulk conduction band with $E_\text{ex}(\text{e}) = 0.51$, 0.43, and 0.16 eV, much higher than the expected excess energies of valence holes $E_\text{ex}(\text{h}) = 0.10$, 0.18, and 0.17 eV, respectively. Taking into account the larger effective mass of the hh band compared to the other valence bands, the transitions yield a higher population due to the excitation channel from hh states. Therefore the mean kinetic energy of excited electrons is much higher than that of holes in the valence band, and the large difference in the mean kinetic energy between the photoexcited electrons and holes is reduced during the energy relaxation processes [23].

Based on the transport of nonthermal carriers, the observed temporal change of SP energy can be described as follows. Before the photoexcitation ($t_d < 0$), band bending is relaxed by populating the SUB with electrons excited by the previous pump pulse. A new pump pulse generates electrons with much larger excess energies in the conduction band and holes with small excess energies in the valence bands. The optical absorption coefficient of the 1.5-eV excitation is about $5 \times 10^4\,\mathrm{cm}^{-1}$ so that the absorption depth is 200 nm [24]. Thus the photoexcitation forms a steep concentration gradient of generated electron-hole pairs near the surface region, which induces the net current of carriers into the bulk. Since the carrier flux (the number of carriers that cross a plane placed normal to the carrier flow) is proportional to the carrier velocity, excited electrons with higher mean velocity causes a significantly higher current of electrons into the bulk compared to the hole current. The resulting charge redistribution induces the downward shift of SP. As t_d increases, the carrier density gradient decreases and photogenerated carriers cool down. In addition, the bulk-to-surface transition can result in a greater reduction in electron density in the near-surface region. Around $t_d = 2\,\mathrm{ps}$, where the SP reaches a minimum, the diffusion current into the bulk can be compensated by the drift current to the surface due to the induced band bending. For larger t_d, the electron drift current from the deep bulk supplies the electron into the near-surface region and moves the SP upward slowly. A similar ultrafast energy shift of SP on a subpicosecond time scale was also observed for the GaAs(100) surface [25]. These results reveal an important role of energetic carriers far from the equilibrium in the ultrafast carrier transport and the resulting change of SP in a ps regime.

V. SUMMARY

We directly imaged the relaxation pathways of photoexcited electrons on the Ge(001)-$c(4 \times 2)$ surface by time- and angle-resolved two-photon photoelectron spectroscopy. Excited surface electrons were found to relax along the surface unoccupied band, and then to accumulate near the band bottom in 4 ps. During the electron relaxation, the SP is shifted, strongly indicating the important role of ultrafast transport of nonthermal carriers. Taking into account the dynamical change of SP, the electronic structure of the surface conduction band has been determined with a high energy and momentum resolution. Although the measured momentum range was limited due to the low photon energy used to probe, the present study is the first to unveil the energy dispersion properties along the three symmetric directions experimentally. The use of probe light with higher photon energies is a promising technique for a complete determination of the band structure over the entire momentum range in the first Brillouin zone.

ACKNOWLEDGMENTS

This work was in part supported by JSPS KAKENHI Grants No. 16K13822 and No. 17H02773.

[1] W. Monch, *Semiconductor Surface and Interfaces* (Springer, Berlin, 1995).
[2] H. Seo, R. C. Hatch, P. Ponath, M. Choi, A. B. Posadas, and A. A. Demkov, Phys. Rev. B **89**, 115318 (2014).
[3] E. Landemark, C. J. Karlsson, L. S. O. Johansson, and R. I. G. Uhrberg, Phys. Rev. B **49**, 16523 (1994).
[4] K. Nakatsuji, Y. Takagi, F. Komori, H. Kusuhara, and A. Ishii, Phys. Rev. B **72**, 241308(R) (2005).
[5] P. E. J. Eriksson, M. Adell, K. Sakamoto, and R. I. G. Uhrberg, Phys. Rev. B **77**, 085406 (2008).
[6] O. Gurlu, H. J. W. Zandvliet, and B. Poelsema, Phys. Rev. Lett. **93**, 066101 (2004).
[7] M. Wojtaszek, R. Zuzak, S. Godlewski, M. Kolmer, J. Lis, B. Such, and M. Szymonski, J. Appl. Phys. **118**, 185703 (2015).
[8] Y. Takagi, Y. Yoshimoto, K. Nakatsuji, and F. Komori, J. Phys. Soc. Jpn. **72**, 2425 (2003).
[9] K. Sagisaka and D. Fujita, Phys. Rev. B **72**, 235327 (2005).
[10] M. Rohlfing, P. Kruger, and J. Pollmann, Phys. Rev. B **54**, 13759 (1996).
[11] P. Kruger, A. Mazur, J. Pollmann, and G. Wolfgarten, Phys. Rev. Lett. **57**, 1468 (1986).
[12] L. Kipp, R. Manzke, and M. Skibovski, Solid State Commun. **93**, 603 (1995).
[13] J. E. Ortega and F. J. Himpsel, Phys. Rev. B **47**, 2130 (1993).
[14] R. Haight and M. Baeumler, Phys. Rev. B **46**, 1543 (1992).
[15] M. Weinelt, M. Kutschera, R. Schmidt, C. Orth, T. Fauster, and M. Rohlfing, Appl. Phys. A **80**, 995 (2005); M. Weinelt, M. Kutschera, T. Fauster, and M. Rohlfing, Phys. Rev. Lett. **92**, 126801 (2004).
[16] T. Ichibayashi and K. Tanimura, Phys. Rev. B **75**, 235327 (2007).
[17] S. Tanaka, T. Ichibayashi, and K. Tanimura, Phys. Rev. B **79**, 155313 (2009).
[18] J. Kanasaki, H. Tanimura, and K. Tanimura, Phys. Rev. Lett. **113**, 237401 (2014).
[19] M. Kolmer, S. Godlewski, H. Kawai, B. Such, F. Krok, M. Saeys, C. Joachim, and M. Szymonski, Phys. Rev. B **86**, 125307 (2012).
[20] J. Kanasaki, I. Yamamoto, J. Azuma, and S. Fukatsu (unpublished).
[21] H. Wormeester, D. J. Wentink, P. L. de Boeij, C. M. J. Wijers, and A. van Silfhout, Phys. Rev. B **47**, 12663 (1993).
[22] P. Y. Yu and M. Cardona, *Fundamentals of Semiconductors: Physics and Materials Properties* (Springer, Berlin, 1996).
[23] U. Hohenester, P. Supancic, P. Kocevar, X. Q. Zhou, W. Kutt, and H. Kurz, Phys. Rev. B **47**, 13233 (1993).
[24] D. E. Aspnes and A. A. Studna, Phys. Rev. B **27**, 985 (1983).
[25] P. Siffalovic, M. Drescher, and U. Heinzmann, Europhys. Lett. **60**, 924 (2002).